HYDROGEN SAFETY

Impact of Release Temperature on Hydrogen Jet Mixing with Ambient Air

RESEARCH

QIANG GE
ZHENBIAO ZHOU
DANIEL CREEDON
YI YANG
MICHAEL J. BREAR
DEEPAK SAINI
JOSEPH D. BERRY
MOHSEN TALEI
RICHARD D. SANDBERG
MELISSA KOZUL

*Author affiliations can be found in the back matter of this article

KIT Scientific Publishing

hySafe
INTERNATIONAL ASSOCIATION FOR HYDROGEN SAFETY

ABSTRACT

Liquid hydrogen leaks produce large volumes of cryogenic, flammable mixtures, posing major safety risks to personnel and equipment. This work studies the impact of hydrogen release temperature on jet mixing and dispersion in ambient air. Controlled release experiments are conducted with dry air in an open-ended chamber, with the hydrogen storage temperature varying from 35 to 290 K while the release pressure or mass flow rate is kept constant. The hydrogen mass fraction and mixture temperature are measured using a sampling probe at 20–255 mm axially and 0–50 mm radially from the release nozzle. For release temperatures between 35 and 129 K, the centreline decay of the hydrogen mass fraction and the mixture enthalpy both become slower as the release temperature decreases. This decay rate, determined using Kleinstein's classic method (Kleinstein, 1964), is between 0.2 and 0.3 for the hydrogen mass fraction, comparable to previous experiments analysed using Chen and Rodi's (1980) method. On the other hand, the radial decay rate of both scalars, characterized by Gaussian functions, increases as the release temperature decreases. While some scattering exists in these trends, the relative decay of the hydrogen mass fraction and the mixture enthalpy, representing the turbulent Lewis number (Le_t), shows a consistent variation with the release temperature. At room temperature Le_t approaches 1, as commonly assumed in CFD simulations of turbulent jet mixing. As the release temperature decreases, Le_t drops approximately linearly and reaches approximately 0.8 at 70 K and even lower at colder release temperatures where Kleinstein's analysis becomes more challenging. These results provide the first experimental data evidencing this slower decay with colder jets, which leads to longer and larger flammable envelopes. The experiments are also simulated using the open-source HyRAM software. While the low-order model reproduces the axial and radial measurements reasonably well at deep cryogenic conditions, the performance deteriorates with increasing release temperature, particularly at room temperatures, likely due to the identical, temperature-invariant decay rates assumed for the hydrogen concentration and the mixture temperature in the model.

CORRESPONDING AUTHOR:
Yi Yang
Department of Mechanical Engineering, University of Melbourne, AU
yiyang.mecheng@unimelb.edu.au

KEYWORDS:
Cryogenic hydrogen release; Turbulent jet mixing; Decay rate; Turbulent Lewis number; Liquid hydrogen safety

TO CITE THIS ARTICLE:
Ge, Q., Zhou, Z., Creedon, D., Yang, Y., Brear, M.J., Saini, D., Berry, J.D., Talei, M., Sandberg, R.D. and Kozul, M. (2026) 'Impact of Release Temperature on Hydrogen Jet Mixing with Ambient Air', *Hydrogen Safety*, 3(1), pp. 284–304. Available at: https://doi.org/10.58895/hysafe.79

DOI: 10.58895/hysafe.79

NOMENCLATURE

Latin Symbols	
a	offset in hyperbolic relations
C_p	mass-based specific heat
$\overline{C}_p$	molar-based specific heat
D	nozzle diameter
H	enthalpy
T	temperature
v	velocity
Y	mass fraction
r	radial distance
z	axial distance
Le	Lewis number
Pr	Prandtl number
Sc	Schmidt number
Re	Reynolds number
Greek Symbols	
κ	axial decay rate
η	radial decay rate
ρ	density
Subscripts	
a	ambient air
∞	ambient
cl	centreline
e	nozzle exit
eq	equivalent of notional nozzle exit
eff	effective
h	enthalpy
mix	mixture
r	storage
t	turbulent
v	velocity
y	mass fraction

1. INTRODUCTION

Hydrogen is attracting major interest as a clean energy carrier and carbon-free fuel. To overcome the low volumetric energy density, hydrogen is commonly stored as a liquid or as a high-pressure gas. The former offers higher density and thus is more suitable for long-distance transport (Yue *et al.*, 2021). Leaks of liquid hydrogen, however, produce high-density, highly flammable mixtures which pose major fire and explosion risks to the surroundings (LaChance *et al.*, 2009; Schefer *et al.*, 2011). An accurate understanding of cryogenic hydrogen dispersion behaviours is therefore essential for LH2 handling, storage and transport (NFPA, 2023).

In the following, we firstly review the general characteristics of underexpanded jets and classic methods for analysis of decay rates, then review existing hydrogen release experiments in laboratory settings in the form of both high-pressure gases and cryogenic fluids, and finally present the objective of this work.

1.1 CHARACTERISTICS OF FREE JET MIXING INTO STILL AIR

Liquid hydrogen can be released as a multi-phase jet or a vapour-only jet. The vapour-only release, typically involved in small leaks, can be characterized by an underexpanded jet, choked at the leak point (Courant and Friedrichs, 1948; Shapiro, 1953). The underexpanded

DOI: 10.58895/hysafe.79

region contains complex shock structures which are typically influenced by the exit geometry and the pressure ratio between the storage and the ambient (Franquet *et al.*, 2015). The intricate interactions of shocks are not essential for the subsequent jet development and are often modelled with notional nozzles that transform the exit flow into a subsonic jet with an equivalent diameter (Birch *et al.*, 1984; Birch *et al.*, 1987; Ewan and Moodie, 1986; Molkov, 2012; Yuceil and Otugen, 2002). The downstream dispersion can then be characterized by a subsonic, turbulent, free jet that exhibits self-similar features as depicted in Figure 1 and analysed below.

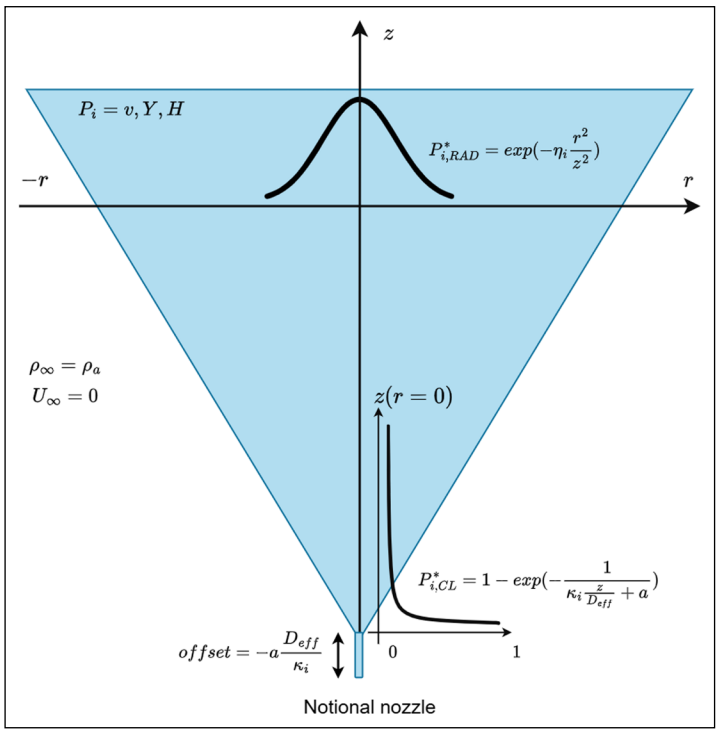

Figure 1 Schematic of scalar dissipation in an ideally expanded jet issued from a notional nozzle. Scalar decay can be described by a hyperbolic function along the axial direction and a Gaussian function along the radial direction (Kleinstein, 1964).

Kleinstein (1964) proposed a method for analysing turbulent, axisymmetric jets by linearization of the governing equations in the von Mise plane, coupled with an eddy viscosity formulation by Ferri, Libby, and Zakkay (1964). The axial decay is represented by a hyperbolic relationship between the decay parameter and the downstream distance, as shown in equation (1) for velocity, mass fraction and mixture enthalpy

$$\frac{v_{cl}}{v_e} = 1 - \exp\left(-\frac{1}{\kappa_v \frac{z}{D_{eff}} + a}\right)$$

$$Y_{cl} = 1 - \exp\left(-\frac{1}{\kappa_y \frac{z}{D_{eff}} + a}\right) \quad (1)$$

$$\frac{H_{cl} - H_\infty}{H_e - H_\infty} = 1 - \exp\left(-\frac{1}{\kappa_h \frac{z}{D_{eff}} + a}\right)$$

where v_{cl} and v_e are the centreline and exit velocity, Y_{cl} is the centreline mass fraction and H_{cl}, H_e and H_∞ are the centreline, exit and ambient enthalpy, respectively. The decay rates are represented by κ, in which subscripts v, y, h refer to velocity, mass fraction and enthalpy, respectively. z is the downstream distance, a is the offset for the virtual origin and D_{eff} is the effective diameter, defined as $D_{eff} = D_{eq}\sqrt{\frac{\rho_{eq}}{\rho_a}}$, where D_{eq} and ρ_{eq} are the equivalent diameter and jet density at the exit of the notional nozzle model, and ρ_a is the ambient air density.

In the far field, this hyperbolic relationship can be reduced to a linear function between the inverse of the scalar and normalized distance (Chen and Rodi, 1980; So and Aksoy, 1993), as shown in equation (2).

DOI: 10.58895/hysafe.79

$$\frac{v_e}{v_{cl}} = k_v \frac{z}{D_{eff}} \quad \frac{1}{Y_{cl}} = k_y \frac{z}{D_{eff}} \quad \frac{H_e - H_\infty}{H_{cl} - H_\infty} = k_h \frac{z}{D_{eff}} \tag{2}$$

All hydrogen release experiments to date have adopted this expression for decay analysis, although the definition of effective diameter was somewhat different among the studies, as summarized in Table 1. Nevertheless, the approximation to equation (1) is only valid for far downstream locations, and errors have been reported for using this formulation in near-nozzle regions (Li *et al.*, 2018; Okabayashi *et al.*, 2019; Takeno *et al.*, 2017).

From the obtained decay rates, dimensionless parameters for turbulent mixing can be derived (Kleinstein, 1964), as shown in equation (3).

$$\frac{\kappa_v}{\kappa_h} = Pr_t, \frac{\kappa_v}{\kappa_y} = Sc_t, \frac{\kappa_h}{\kappa_y} = Le_t \tag{3}$$

The turbulent parameters can be derived from ratios between different κ. Specifically, Pr_t represents the relative decay rate of velocity and enthalpy, Sc_t the ratio between velocity and mass fraction and Le_t the ratio between enthalpy and mass fraction decay rates (Kleinstein, 1964). Two out of the three are required to define the system.

On the radial direction, the scalar decay is described by a Gaussian distribution (equation (4))

$$\frac{v}{v_{cl}} = \exp\left(-\eta_v \frac{r^2}{z^2}\right) \quad \frac{Y}{Y_{cl}} = \exp\left(-\eta_y \frac{r^2}{z^2}\right) \quad \frac{H - H_\infty}{H_{cl} - H_\infty} = \exp\left(-\eta_h \frac{r^2}{z^2}\right), \tag{4}$$

where the decay rates are represented by the Gaussian coefficient η, and r is the radial distance (Corrsin and Uberoi, 1949; Chen and Rodi, 1980; Kleinstein, 1964). Kleinstein's analysis yielded a comparable expression to the same effect. Similarly, turbulent mixing parameters can be derived for the radial direction from η (equation (5))

$$\frac{\eta_h}{\eta_v} = Pr_t, \frac{\eta_y}{\eta_v} = Sc_t, \frac{\eta_y}{\eta_h} = Le_t \tag{5}$$

1.2 COMPRESSED ROOM-TEMPERATURE HYDROGEN JET MIXING IN STILL AIR

Hydrogen releases at room temperature have been reported by Ruggles and Ekoto (2012) at Sandia. They conducted vertical releases at stagnation conditions of 9.83 bar and 296 K through a 1.5-mm diameter orifice. Rayleigh scattering was used to obtain the mole fraction of hydrogen. The centreline mass fraction decay rate was determined to be 0.214 with static air and 0.222 with 0.5 m/s co-flow air (Ruggles, 2015). The experiment also measured radial mass fraction data, and by normalizing with the centreline value, all radial mass fraction distributions were characterized by a single Gaussian function with a coefficient η of 59. This value matched an earlier study of helium, methane and propane releases at room temperature (Richards and Pitts, 1993).

Horizontal room temperature releases were reported by Ruffin, Mouilleau and Chaineaux (1996) at 40 bar with 25–100 mm nozzles. The centreline mass fraction decay rate was found to be 0.27, with the downstream distance normalized by the notional nozzle equivalent exit diameter and density (Birch *et al.*, 1984). Other horizontal room-temperature releases reported the centreline mass fraction decay rates around 0.3 (Okabayashi *et al.*, 2019; Takeno *et al.*, 2017), which are higher than those from vertical experiments, but similar to those from cryogenic horizontal releases by Veser *et al.* (2011).

1.3 CRYOGENIC HYDROGEN JET MIXING IN STILL AIR

Friedrich *et al.* (2012) from Karlsruhe Institute of Technology conducted vertical hydrogen releases at temperatures from 34 to 65 K and pressures from 7 to 35 bar using 0.5 and 1 mm nozzles. The lowest measurement is 40 mm above the release point. Background Oriented Schlieren (BOS) technique was used to determine the density gradient. The centreline hydrogen concentration was calculated using the density gradient and temperature measurement (with thermocouples) at different downstream locations. The centreline mass fraction decay rate was obtained from the concentration profiles to be 0.233 using equation (2), where the effective nozzle diameter was obtained using the exit diameter and hydrogen storage density.

Hecht and Panda (2019) conducted vertical cryogenic hydrogen releases at Sandia National Laboratory with the release condition of 48 to 63 K and 2–5 bar using 1 and 1.25 mm nozzles. Their work reported the only set of data for concentration and temperature along both axial and radial directions. Raman scattering was used to determine the hydrogen and nitrogen (air) concentrations using two cameras, where the gas temperature was calculated using the ideal gas law. The lowest measurement is 38 mm above the release point. Based on their published data, the measurement uncertainty is estimated to be ±5 mol% for hydrogen from 40 to 80 mol% and ±20 K for temperature from 100 to 210 K. The axial mass fraction decay rate was reported to be 0.277, where the downstream distance is normalized with the exit diameter and hydrogen storage density. The axial decay rate for the normalized temperature is nearly one order of magnitude smaller, 0.0281. In the radial direction, the mass fraction and temperature both follow a Gaussian distribution (equation (4)), and a single Gaussian coefficient can describe the decay of a given scalar at different axial locations, for example, η = 49 and 42 for hydrogen mass fraction and mixture temperature, respectively. A later paper reanalysed the Raman results (Li *et al.*, 2023) by reducing the measurement noise and reported lower axial decay rates, 0.22 and 0.023 for mass fraction and temperature, respectively. The Gaussian coefficient for the radial temperature profile was also updated to be 50, whereas that for the radial mass fraction profile remained as 49. These updated decay rates matched more closely with hydrogen mass fraction results from previous room-temperature release experiments (Richards and Pitts, 1993; Ruggles, 2015) reviewed above.

Veser *et al.* (2011) conducted horizontal cryogenic hydrogen releases with storage pressures of 8.25–68.5 bar and release temperatures of 35, 80 and 290 K using round nozzles of 1, 2 and 4 mm diameter at Forschungszentrum Karlsruhe (FZK) facilities. They found buoyancy playing a significant role in the axial decay of velocity and hydrogen concentration and reported a larger centreline mass fraction decay rate (0.313) than those with vertical release.

A summary of laboratory hydrogen release experiments reviewed is provided in Table 1.

Table 1 Release conditions, measurement methods and centreline decay rates of past hydrogen release experiments.

P: measured scalar; *P**: normalized scalar, definition in equation (2); D_{eq}: equivalent diameter (notional nozzle exit); D_e: nozzle diameter; ρ_e: density at the nozzle exit; ρ_{eq}: equivalent density at notional nozzle exit; ρ_a: ambient air density; ρ_r: storage density.

*Horizontal release.

**Hydrogen analysed offline, sensor type not reported.

EXPERIMENT	RELEASE TEMPERATURE AND PRESSURE	NOZZLE DIAMETER (mm)	MEASURED PARAMETER (*P*)	MEASUREMENT METHOD	EFFECTIVE NOZZLE SIZE (D_{eff})	CENTRELINE DECAY RATE (P^{*-1} VS. Z/D_{eff}) (EQUATION (2))
Friedrich *et al.* (2012)	34–65 K 7–35 bar	0.5, 1	Mass fraction	BOS and thermal couples	$D_e\sqrt{\frac{\rho_r}{\rho_a}}$	0.233
Hecht and Panda (2019)	48–61 K 2–5 bar	1, 1.25	Mass fraction, mixture temperature	Raman scattering	$D_e\sqrt{\frac{\rho_r}{\rho_a}}$	0.277 (mass) 0.0281 (temp)
					$D_e\sqrt{\frac{\rho_e}{\rho_a}}$ reanalysis with noise reduction (Li *et al.*, 2023)	0.22 (mass) 0.023 (temp)
Veser *et al.* (2011)*	35, 80 and 290 K 5–60 bar	1, 2, 4	Velocity, mass fraction	PIV and Sampling probe**	$D_e\sqrt{\frac{\rho_e}{\rho_a}}$	0.193 (velocity) 0.313 (mass)
Ruggles, (2015) and Ruggles and Ekoto (2012)	296 K 10 bar	1.5	Mass fraction	Rayleigh scattering	$D_e\sqrt{\frac{\rho_e}{\rho_a}}$	0.214 (Ruggles, 2015) 0.222 (Ruggles and Ekoto, 2012)
Ruffin, Mouilleau and Chaineaux (1996)*	288 K 40 bar	25	Mass fraction	Pellistor hydrogen sensor	$D_{eq}\sqrt{\frac{\rho_{eq}}{\rho_a}}$	0.27

CFD and low-order models have been used to simulate these experiments. A common assumption in the CFD simulations is the turbulent Prandtl number (Pr_t) and Schmidt number (Sc_t) being equal (Giannissi and Venetsanos, 2018; Giannissi *et al.*, 2021; Saini *et al.*, 2024), which by definition set the turbulent Lewis number (Le_t) to unity. Kleinstein (1964) applied equation (4) to room-temperature helium/air jets and yielded a Pr_t of 0.715 and Sc_t of 0.708, giving a Le_t of 0.99. Similar studies for hydrogen/air jets or cryogenic jets have not been reported.

1.4 OBJECTIVE OF THIS WORK

Cryogenic hydrogen can be released at a temperature well below that for air condensation, which significantly alters the thermodynamic and transport properties of involved gases, affects the heat/mass transfer and subsequently impacts the jet dispersion (Hu *et al.*, 2023; Matheis *et al.*, 2020; Traxinger Banholzer and Pfitzner, 2018). From the review above, a systematic investigation of the impact of release temperature on hydrogen dispersions has not been reported. Among the few experiments for cryogenic hydrogen release, most have reported only the concentration in the axial direction where the measurements bear significant uncertainties from the optical methods used (Friedrich *et al.*, 2012; Hecht and Panda, 2019). The impact of release temperature has been studied only by comparing data from different experiments, limiting the accuracy of the comparison.

To address this gap, this work conducts independent hydrogen concentration and mixture temperature measurements for both cryogenic and room-temperature releases in a single experimental setup. We use a movable sampling probe with two degrees of freedom to measure the decay of hydrogen mass fraction and enthalpy along both the axial and radial directions over a wide range of release temperatures, pressures, and mass flow rates. These decay rates are compared with data from the literature as well as simulation results using a low-order model, HyRAM+ 6.0 (Ehrhart *et al.*, 2025). The treatment of Kleinstein (1964) is adopted to derive turbulent transport parameters, from which the impact of release temperature on hydrogen jet mixing is elucidated.

2. METHODOLOGY

2.1 CRYOGENIC RELEASE FACILITY

Figure 2 shows a schematic of the hydrogen release facility at the University of Melbourne. The main components include a cryogenic heat exchanger and a release chamber. The heat exchanger uses three-stage cooling, a similar design to that in the Sandia experiment (Hecht and Panda, 2019; Panda and Hecht, 2017). The first stage uses a liquid nitrogen bath to cool the room temperature hydrogen (in coil flow) to around 80 K. The second stage is a counter-flow heat exchanger which uses the boil-off helium from the third stage to cool hydrogen to approximately 40 K. The third stage uses a liquid helium bath to cool the hydrogen further down to approximately 30 K. The temperatures at the inlets of the first and second stages and the outlet of the third stage are monitored using silicon diodes (Lakeshore DT-670). Liquid hydrogen and liquid helium are supplied from the respective dewars with the liquid level monitored with level sensors. The system is designed for a hydrogen flow rate up to 1 g/s and an operating pressure up to 10 bar.

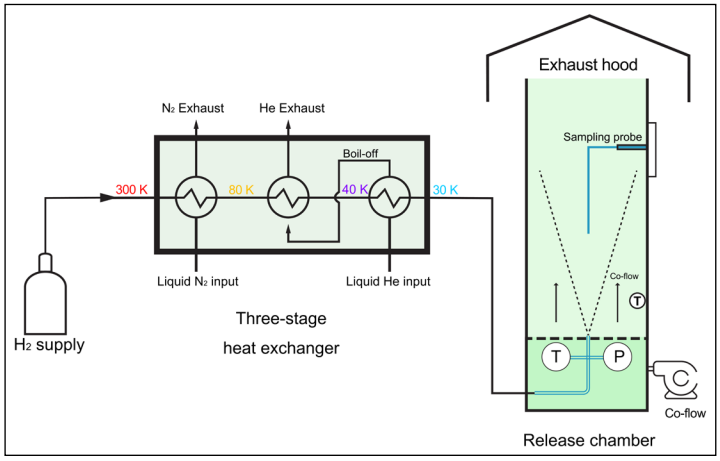

Figure 2 Schematic of the hydrogen release facility.

A vacuum-jacketed transfer hose connects the heat exchanger outlet to the release chamber. The hose is fitted with a silicon diode temperature sensor (Lakeshore DT-670) and a pressure transducer (Omega PXM519-010BAS2IS), which is installed at 68 mm upstream of the release orifice to indicate the storage temperature and pressure. Round-shaped orifices of 0.75, 1 and 1.25 mm diameter are used. The orifice was drilled into a stainless steel plate of 20 mm diameter and 0.73 mm thickness bolted to the end of the transfer hose.

DOI: 10.58895/hysafe.79

The release chamber has a cross-section of 0.5 m by 0.5 m and a height of 2.5 m. The orifice is located at the centre of the base plane. Air co-flow is supplied from the bottom through a honeycomb panel (flush with the orifice exit) to provide a consistent chamber environment for different release conditions. To circumvent icing from air moisture, dry air is used for all releases reported here (cryogenic and room-temperature). The air is supplied from a 50-bar compressor with a refrigeration dryer at a flow rate of 30 g/s, giving an average co-flow velocity of 0.1 m/s. The relative humidity of the co-flow is 5–7%, measured using a humidity sensor underneath the honeycomb. The hydrogen/air mixture is extracted via a fume hood (0.9 m by 0.9 m) above the release chamber, which dilutes the mixture below the lower flammability limit (4 vol%) before entering the lab exhaust system. Thermocouples are installed inside the chamber to detect any ignition event, which will shut down the hydrogen flow and trigger an emergency response.

A sampling probe is installed inside the release chamber to measure hydrogen mole fraction and gas temperature. The probe is made of an ultra-low thermal conductivity material, G10, with a 3-mm inner diameter and 1-mm thickness. The probe is installed on a linear traverse platform (Zaber X-LRT-EC) with two degrees of freedom. From the release point, the probe can move from 20-1500mm along the vertical direction and 0–50 mm along the horizontal direction. The temperature is measured with a silicon diode sensor (Lakeshore DT-670) installed inside the G10 tube flush with the probe inlet. The hydrogen mole fraction is measured with a thermal conductivity detector (XEN-5320-HP-USB) installed approximately 800 mm away from the probe inlet. A gas sample is pulled past the sensor and through the tube by a small vacuum generator mounted on the stage of the linear traverse. This vacuum generator is based on the Venturi effect and operated with a small air flow. The analyser has an absolute uncertainty of ±2 vol% and a response time of less than one second. The silicon diode sensor has an uncertainty of ±0.5 K between 2 and 305 K. Measurement and control are realized via an in-house LabVIEW program.

For each release, Schlieren imaging is employed at the beginning to check the verticality of the released jet. After this is verified, a 'symmetry test' is conducted, which measures the hydrogen mole fraction and temperature at symmetrical radial positions and 20, 30 and 40 mm above the nozzle, to ensure that the probe is positioned at the centre of the jet.

The presence of the sampling probe can induce bias in the concentration and temperature measurements. Existing literature suggests limited impact on the upstream velocity (within 1–2 probe diameters) (Olshefski *et al.*, 2022; Schlichting and Gersten, 2017) and a small bias on composition measurements (Bilger and Beck, 1975; Kent and Bilger, 1973; Lupant, Pesenti, and Lybaert, 2010). This probe-induced bias is assumed to be covered in the H_2 sensor's stated absolute uncertainty (±2%) in this work, which is subject to further investigations.

2.2 RELEASE CONDITIONS

Two sets of experiments are conducted to investigate the effect of release temperature on hydrogen dispersion. The first uses constant storage pressure, which sets the pressure ratio and jet velocity, the most important parameters affecting the underexpanded jet in the near field. Storage pressures at approximately 3 and 5 bar are investigated. The second set uses a constant mass flow rate (0.30, 0.36, 0.43 g/s), which sets the jet Reynolds number, the primary parameter controlling the jet decay and turbulent mixing. Due to the significant variation in hydrogen's viscosity at cryogenic temperatures, the Reynolds number decreases with the storage temperature. Tables 2 and 3 list the conditions for the temperature sweep at fixed pressures and fixed mass flow rates, respectively. The mass flow rates of hydrogen were measured using a Coriolis flowmeter before the heat exchanger. Also reported is the calculated mass flow rate for choked flow using the storage conditions and thermodynamic properties from the REFPROP database (Lemmon, Huber and McLinden, 2013). The discrepancy between the two flow rates can be attributed to the discharge coefficient, as well as the uncertainty in measuring the storage temperature, pressure and orifice diameter. A similar discrepancy was also reported in Panda and Hecht (2017). Additional release cases not falling into these two sets are reported in the Supplementary Materials.

The notional nozzle model by Yuceil and Otugen (2002) is used in this work. The model considers mass, momentum and energy conservation, as well as the atmospheric pressure at the nozzle exit. For the decay rate evaluation, the axial distance is normalized by $D_{eq}\sqrt{\frac{\rho_{eq}}{\rho_a}}$ as defined in equation (1).

DOI: 10.58895/hysafe.79

TEST #	NOMINAL RELEASE PRESSURE (kPa)	*P* (kPa)	*T* (K)	*D* (mm)	D_{eff} (mm)	JET REYNOLDS NUMBER (*Re*)* 10^5	MEASURED MASS FLOW RATE (g/s)	CALCULATED MASS FLOW RATE (g/s)*
1	300	294	35	1	1.02	4.15	0.43	0.46
4		294	48	1	1.02	2.54	0.36	0.38
7		298	70	1	1.03	1.47	0.29	0.32
12		301	119	1	1.03	0.70	0.21	0.24
17		297	290	1	1.04	0.21	0.13	0.15
6	500	484	69	1	1.13	2.47	0.48	0.52
9		506	103	1	1.14	1.46	0.40	0.44
13		509	126	1	1.15	1.07	0.34	0.39
15		498	289	1	1.18	0.37	0.22	0.25

Table 2 Storage conditions for the release temperature test at fixed release pressure.

* The calculated mass flow rate assumes choked flow using the nozzle diameter and upstream temperature and pressure of the nozzle. Same for Table 3.

TEST #	NOMINAL MASS FLOW RATE (g/s)	*P* (kPa)	*T* (K)	*D* (mm)	D_{eff} (mm)	JET REYNOLDS NUMBER (*Re*)* 10^5)	MEASURED MASS FLOW RATE (g/s)	CALCULATED MASS FLOW RATE (g/s)
7	0.30	298	70	1	1.03	1.47	0.29	0.32
11		409	108	1	1.09	1.08	0.3	0.35
14		627	290	1	1.27	0.50	0.3	0.32
4	0.36	294	48	1	1.02	2.54	0.36	0.38
10		468	105	1	1.12	1.31	0.36	0.4
18		747	290	1	1.35	0.60	0.36	0.38
1	0.43	294	35	1	1.02	4.15	0.43	0.46
8		561	101	1	1.17	1.63	0.44	0.49
16		959	289	1	1.48	0.71	0.43	0.47

Table 3 Storage conditions for the release temperature test at fixed mass flow rates.

3. RESULTS AND DISCUSSION

3.1 AXIAL DECAY

3.1.1 Temperature sweep with fixed storage pressure

Figure 3 shows the centreline hydrogen molar fraction and mixture temperature as a function of axial distance at 300 kPa and 35–290 K. Both properties decrease rapidly near the nozzle and then approach a plateau with a gentler decay. Figure 4 shows the corresponding results at 500 kPa and 69–289 K. Error bars are included to account for sensor measurement uncertainties.

The hyperbolic decay of centreline mass fraction and normalized mixture enthalpy is shown in the subplots c and d in Figures 3 and 4. The hydrogen mass fraction correlates nearly perfectly with the normalized distance, as indicated by the R^2 values. In the hyperbolic relation, κ_y represents the mass fraction decay rate in the axial direction. The virtual origin a is a fitted parameter and varies at each condition. The mass fraction decay rate ranges from 0.18 to 0.25, showing an increasing trend with release temperature (at both 300 and 500 kPa), although the trend is not preserved at room temperature. The decay rates fall into a similar range to those reported in previous studies (Table 1) calculated using the simplified correlation equation (2).

Correlation for the normalized mixture enthalpy decay uses the same offset as the corresponding mass fraction decay, assuming an equal origin for the mass and thermal mixing, as also used in Kleinstein's study (1964). The hyperbolic correlation works excellently for cases above 50 K, where the enthalpy decay rate κ_h shows an increasing trend with the release temperature, similar to κ_y but with a consistently lower value. The correlation does work well for the 48 K case and not at all for the 35 K case, both at 300 kPa. This could be related to the non-monotonic variation of mixture enthalpy along the mixing process, as explained in the following.

DOI: 10.58895/hysafe.79

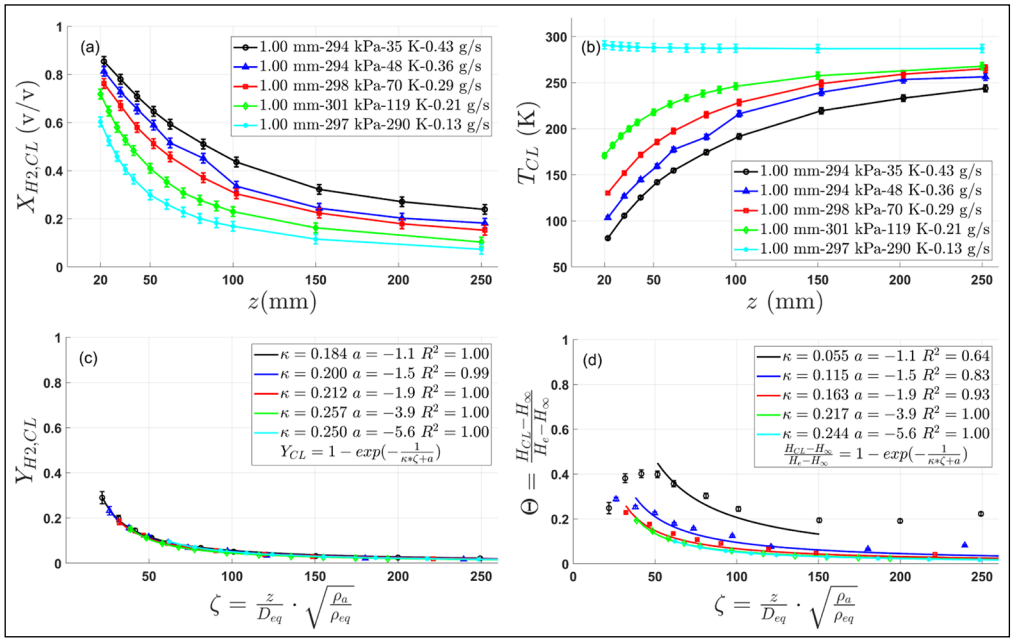

Figure 3 Centreline decay at the release temperature of 35–290 K and a fixed release pressure of 300 kPa: **(a)** hydrogen mole fraction, **(b)** mixture temperature, **(c)** hydrogen mass fraction decay correlation and **(d)** normalized mixture enthalpy decay correlation.

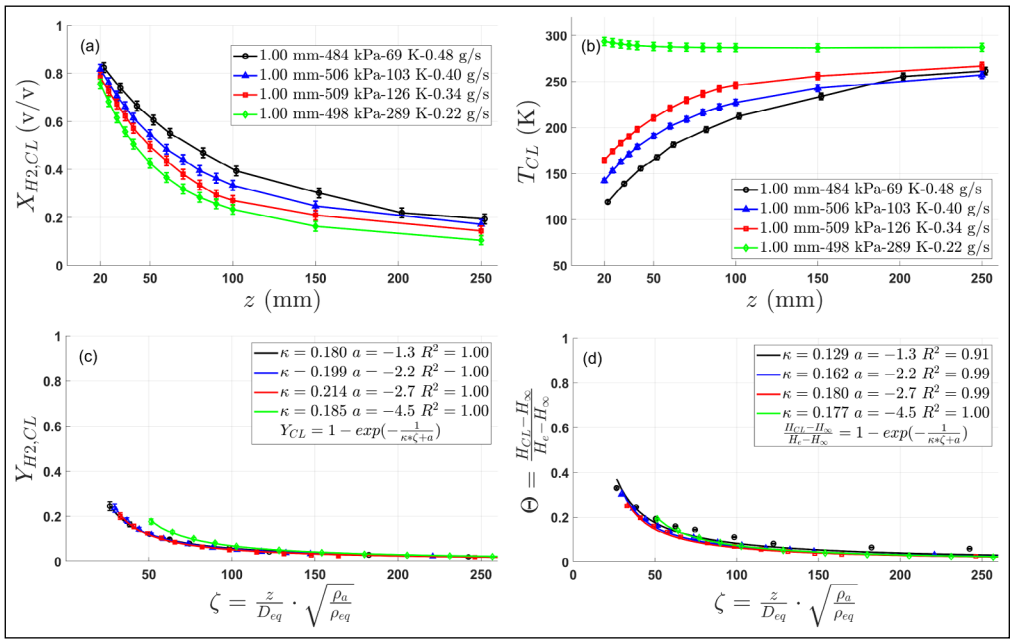

Figure 4 Centreline decay at the release temperature of 69–289 K and a fixed release pressure of 500 kPa: **(a)** hydrogen mole fraction, **(b)** mixture temperature, **(c)** hydrogen mass fraction decay correlation and **(d)** normalized mixture enthalpy decay correlation.

Mixture enthalpy here is calculated using the measured gas temperature and mass fraction (equation (6)).

$$H_{mix} = \left[YC_{pH_2,mix} + (1-Y)C_{p_{air,mix}} \right] T_{mix}, \tag{6}$$

where $C_{p,H2}$ and $C_{p,air}$ are the mass-based specific heat of pure H_2 and air, respectively, at the mixture temperature (T_{mix}) from REFPROP (Lemmon, Huber and McLinden, 2013). The subscript *mix* refers to the mixture of hydrogen and air. Figure 5(a) shows the mixture C_p as a function of temperature and hydrogen fraction, with the 3-bar release cases at 35–290 K included as an example. Since the mass-based C_p of hydrogen is much larger than that of air, the mixture C_p decreases as the hydrogen concentration decreases, which occurs simultaneously as the mixture temperature increases. For the 35 and 50 K release cases, the net result is a non-monotonic variation of mixture enthalpy with temperature, as shown in Figure 5(b). This unusual behaviour causes a problem in analysing the enthalpy decay with Kleinstein's method, which requires monotonic variation of the dimensionless flow properties, for example, those on the left-hand side of equation (1), from 1 (jet) to 0 (far field). While this is true for velocity and mass fraction, it is not the case for mixture enthalpy. For the 35 K release case, two local extreme values are noted, a maximum at 140 K and a minimum at 230 K, which challenges the application of the hyperbolic function to the problem.

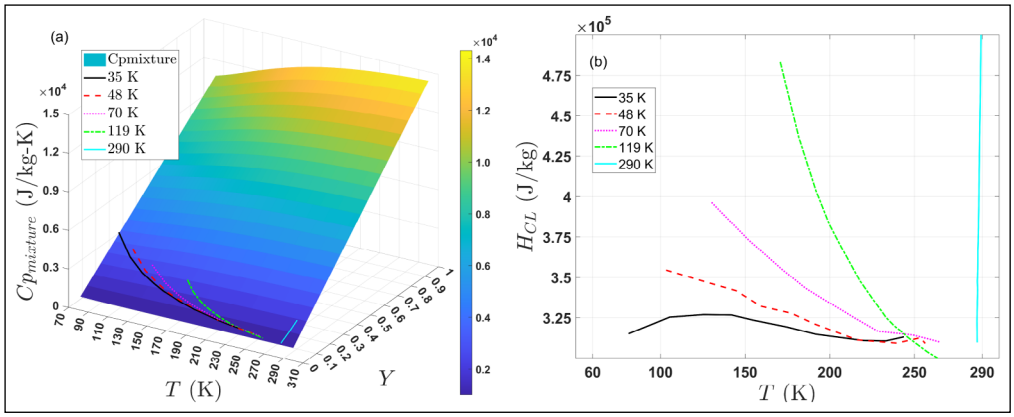

Figure 5 (a) Mixture mass-based C_p as a function of hydrogen mass fraction and mixture temperature. The lines represent the mixture C_p along the centreline for releases at 35–290 K; **(b)** centreline mixture enthalpy (H_{CL}) as a function of mixture temperature for releases at 35–290 K.

One physical reason for the non-monotonicity of the coldest cases could be air condensation near the nozzle, which has been observed by Mie scattering in the 35 and 48 K cases (to be published in a future paper). The heat released from the phase change could alter the local mixture enthalpy, degrading the fit of the centreline decay equation (equation (1)).

3.1.2 Temperature sweep with fixed mass flow rate

Figures 6–8 show the centreline decay at constant mass flow rates of 0.30, 0.36 and 0.43 g/s with different release temperatures. The mass fraction decay is fitted excellently with Kleinstein's method. The enthalpy decay also fits very well, except for the two deep cryogenic cases at 35 and 48 K discussed above. The increasing trend in κ_y and κ_h with release temperature is generally observed among the cryogenic cases, which is disrupted at room temperatures. Similar to the fixed pressure cases, the decay of enthalpy is slower than that of mass fraction along the centreline at corresponding conditions.

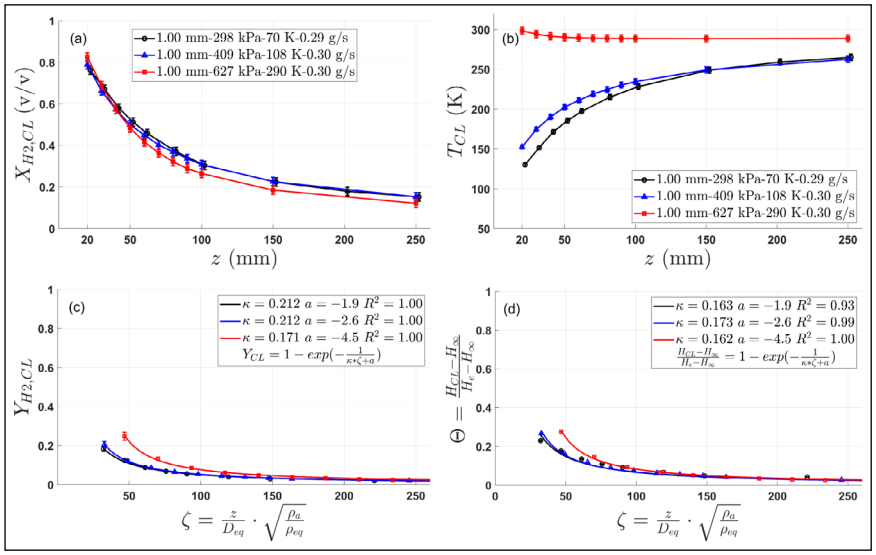

Figure 6 Centreline decay at the release temperature of 70–290 K and a fixed mass flow rate of 0.30 g/s: **(a)** hydrogen mole fraction, **(b)** mixture temperature, **(c)** hydrogen mass fraction decay correlation and **(d)** normalized mixture enthalpy decay correlation.

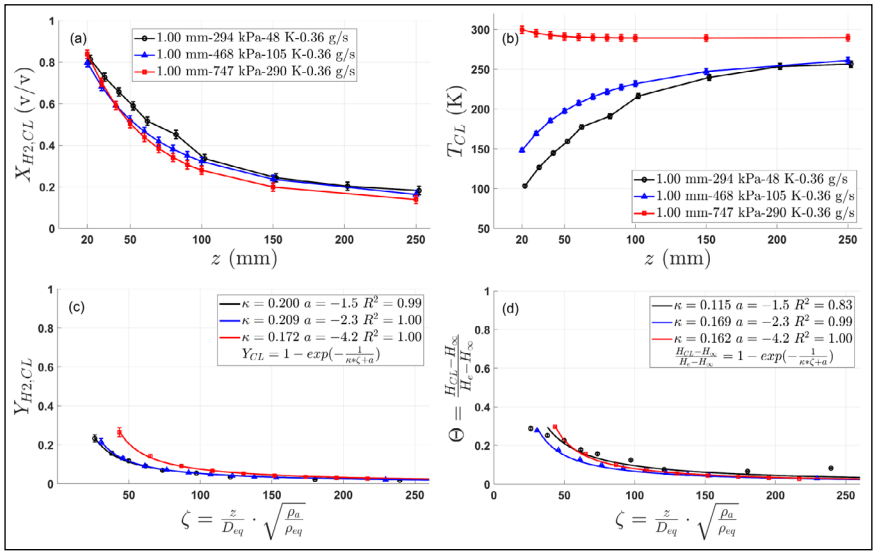

Figure 7 Centreline decay at the release temperature of 48–290 K and a fixed mass flow rate of 0.36 g/s: **(a)** hydrogen mole fraction, **(b)** mixture temperature, **(c)** hydrogen mass fraction decay correlation and **(d)** normalized mixture enthalpy decay correlation.

DOI: 10.58895/hysafe.79

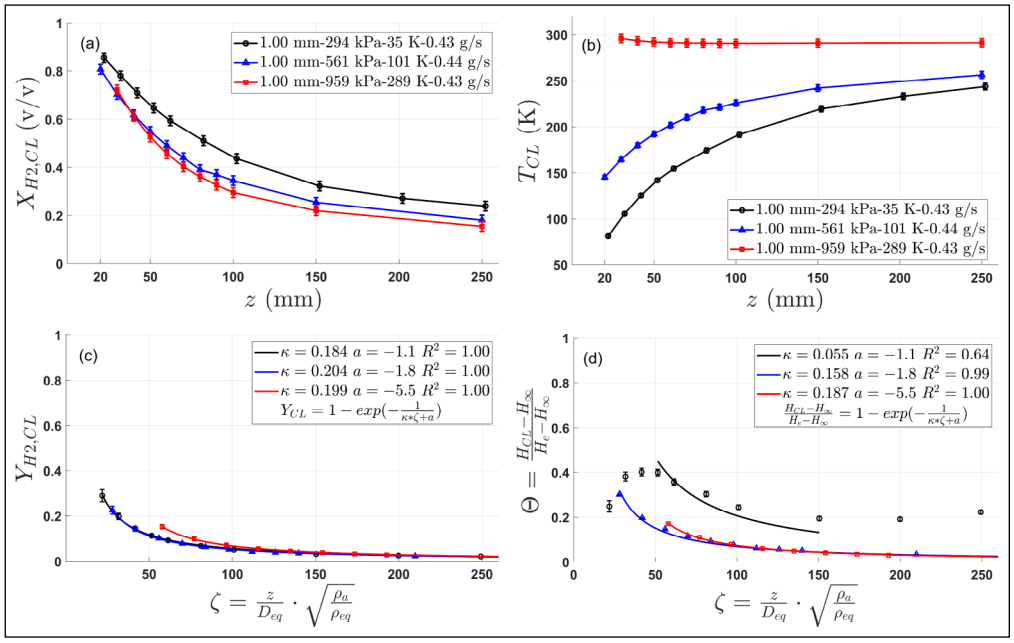

Figure 8 Centreline decay at the release temperature of 35–289 K and a fixed mass flow rate of 0.43 g/s: **(a)** hydrogen mole fraction, **(b)** mixture temperature, **(c)** hydrogen mass fraction decay correlation and **(d)** normalized mixture enthalpy decay correlation.

To evaluate the parameters influencing the axial decay, κ_y and κ_h are plotted against release temperature for all data obtained in this work and those from the literature (Table 1). The dependence on jet Reynolds number is also plotted for comparison. Figure 9 shows that for the data measured in the current study, the mass fraction decay rate exhibits an apparent increasing trend with release temperature for cryogenic release cases (35–119 K), as well as a slightly decreasing trend with jet Reynolds number overall. These trends are more evident with the enthalpy decay rate. The dependence on jet Reynolds number seems counterintuitive but can be explained by the fact that the highest R_e cases are those with the lowest release temperature. Both figures are therefore consistent and indicate that the release temperature is important in determining the scalar decay, in particular, a colder release temperature leading to slower mixing in the axial direction.

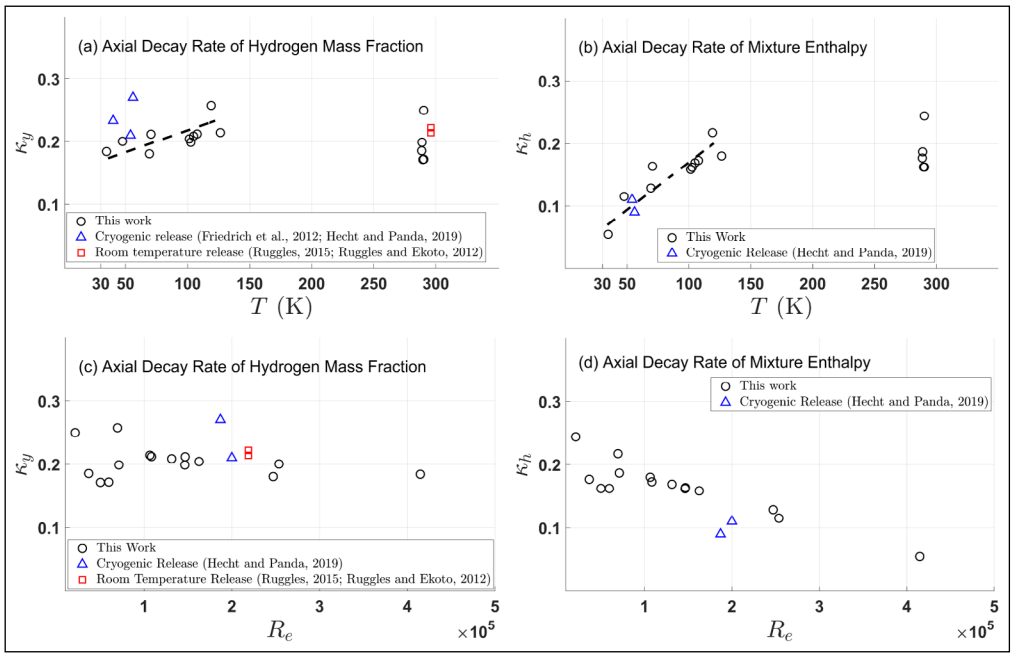

Figure 9 Centreline decay rate of mass fraction and enthalpy as a function of release temperature **(a, b)** and jet Reynolds number **(c, d)**. Experimental data from this work (black circles), cryogenic literature data (blue triangles) (Friedrich *et al.*, 2012; Hecht and Panda, 2019), room temperature literature data (red squares) (Ruggles, 2015; Ruggles and Ekoto, 2012). The dashed line in **(a)** and **(b)** indicates the trend of decay rate for the cryogenic jets measured in this work.

3.2 RADIAL DECAY

The radial distribution of hydrogen mass fraction and mixture enthalpy was measured at 50–100 mm above the nozzle. The measurements are considered in the self-similar region, where the scalar distribution follows the Gaussian function (Chen and Rodi, 1980; Hecht and Panda, 2019; Kleinstein, 1964; Ruggles, 2015). Figure 10 shows the Gaussian profiles for the release temperature sweep with a constant release pressure of 300 kPa, where the scalar is normalized by the centreline value, and the radial distance is normalized by the axial location

DOI: 10.58895/hysafe.79

where the measurement is conducted. Overall, a good fit is obtained for both the mass fraction and enthalpy dispersion. It is worth noting that for some release conditions, the minimum mixture enthalpy is not in the far field but closer to the jet, due to the non-monotonic variation discussed above. In these cases, the normalization uses the smallest enthalpy as H_∞. This change had a minimal impact on the final Gaussian coefficients reported, as points further away from the centreline have a smaller weight on the fitting.

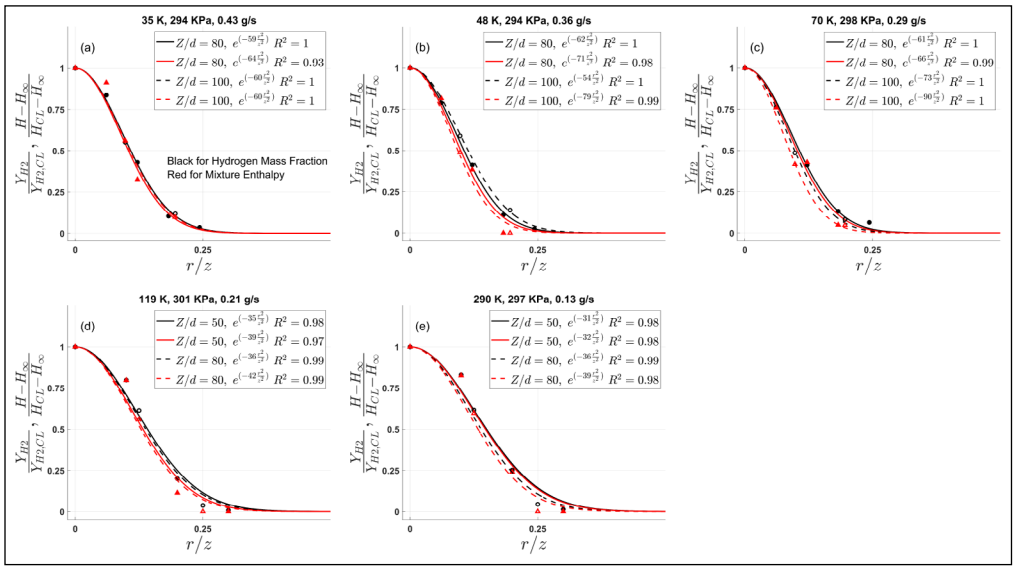

Figure 10 Radial decay of hydrogen mass fraction and mixture enthalpy at different release temperatures and a fixed release pressure of 300 kPa. **(a)** 35 K, **(b)** 48 K, **(c)** 70 K, **(d)** 119 K and **(e)** 297 K; black markers and lines represent normalized mass fraction, and red markers and lines represent normalized mixture enthalpy; different line types signify different downstream locations.

Table 4 summarises the radial decay rates for the temperature sweep at 300 and 500 kPa and those at fixed mass flow rates. The figures for the other conditions are reported in the Supplementary Materials. Within each dataset, the Gaussian coefficients do not show a clear dependence on the release temperature. On the other hand, the decay rates of mass fraction and enthalpy are similar in each case, but the former is consistently smaller by a small margin, except for the 35 K and 48 K cases.

Table 4 Table for all radial decay Gaussian coefficients.

TEST #	RELEASE TEMPERATURE (K)	RELEASE PRESSURE (KPa)	RELEASE MASS FLOW RATE (g/s)	MASS FRACTION η_y				ENTHALPY DECAY η_y			
				DOWNSTREAM LOCATION OF MEASUREMENTS (mm)							
				50	80	90	100	50	80	90	100
Fixed pressure 300 KPa											
1	35	294	0.43		59		60		64		60
4	48	294	0.36		62		54		71		79
7	70	298	0.29		61		73		66		90
12	119	301	0.21	35	36			39	42		
17	290	297	0.13	31	36			32	39		
Fixed pressure 500 KPa											
6	69	484	0.48		38		34		38		38
9	103	506	0.40	39	42			40	43		
13	126	509	0.34	22	18			23	22		
15	289	498	0.22	48	46			50	49		
Fixed mass flow rate of 0.30 g/s											
7	70	298	0.29		61		73		66		90
11	108	409	0.30		40	42	40		44	50	50
14	290	627	0.30	37	40	37	38	38	41	38	39

(Contd.)

TEST #	RELEASE TEMPERATURE (K)	RELEASE PRESSURE (KPa)	RELEASE MASS FLOW RATE (g/s)	MASS FRACTION η_y				ENTHALPY DECAY η_y			
				DOWNSTREAM LOCATION OF MEASUREMENTS (mm)							
				50	80	90	100	50	80	90	100
Fixed mass flow rate of 0.36 g/s											
4	48	294	0.36		62		54		71		79
10	105	468	0.36		44	46	45		49	54	57
18	290	747	0.36	37	38	35	36	38	39	36	37
Fixed mass flow rate of 0.43 g/s											
1	35	294	0.43		59		60		64		60
8	101	561	0.44		37	38	35		40	47	42
16	289	959	0.43		44	43	41		46	43	42

Figure 11 plots the Gaussian coefficients as a function of release temperature and jet Reynolds number for all cases investigated. Additional data from the literature for mass fractions are also included.[1] Among the cryogenic cases, an apparent decreasing trend with increasing release temperature is observed for both η_y and η_h, indicating faster mixing at decreased release temperature. However, the room temperature cases do not follow this trend. This is consistent with the axial results above, although significant scattering exists. On the Reynolds number scale, no clear trend can be identified, suggesting Reynolds number does not play a significant role in the radial decay.

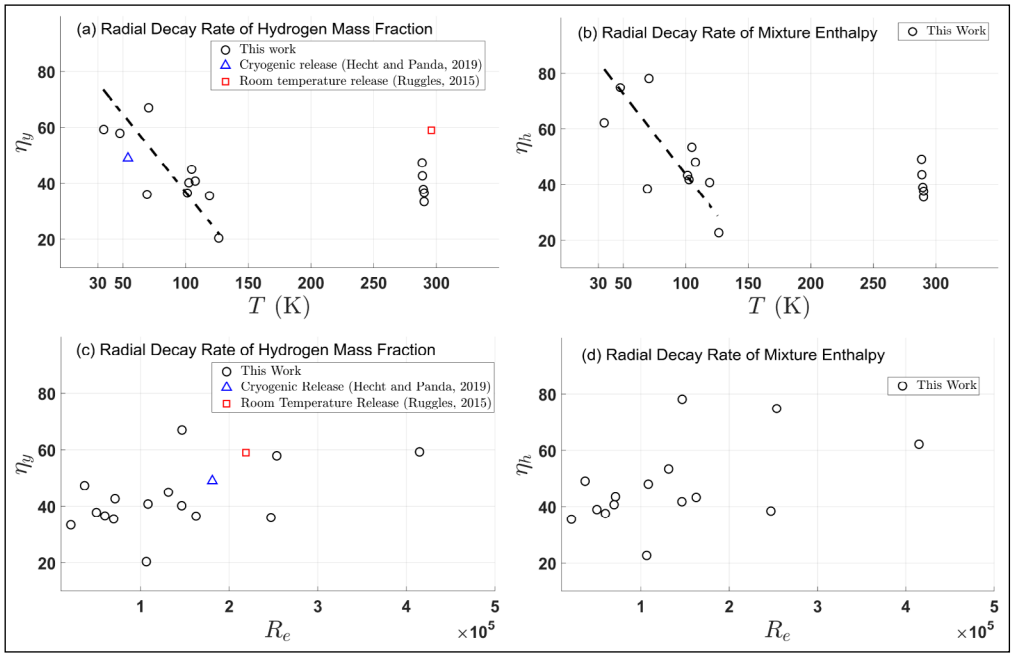

Figure 11 Radial decay rate of mass fraction and enthalpy as a function of release temperature **(a, b)** and jet Reynolds number **(c, d)**. Experimental data from this work (black circles), cryogenic literature data (blue triangles) (Hecht and Panda, 2019), room temperature literature data (red squares) (Ruggles, 2015). The dashed line in (a) and (b) indicates the trend of decay rate for the cryogenic jets measured in this work.

3.3 ESTIMATION OF TURBULENT TRANSPORT PARAMETERS

According to Kleinstein's analysis, the ratio of the axial decay rates of dimensionless velocity and normalized mixture enthalpy can be interpreted as Pr_t. Similarly, the ratio of dimensionless velocity and mass fraction represents Sc_t. Since this work did not measure the jet velocity, we estimate the Le_t along the axial direction using the decay rate ratio of mixture enthalpy and mass fraction, that is, $\frac{\kappa_h}{\kappa_y}$. The result is shown in Figure 12(a) and (c) as a function of the release temperature and jet Reynolds number, respectively. A linear fitting is proposed, excluding the 35 and 48 K cases, which are not in conformity with the hyperbolic relations (equation (1)). In the radial direction, Kleinstein's treatment showed that the ratio of the Gaussian coefficient for

1 Attempts have been made to determine the enthalpy decay for the Sandia experiments (Hecht and Panda, 2019); however, fitting the radial distribution with the Gaussian function yielded $R^2 < 0.7$, likely due to the cryogenic conditions and measurement uncertainty. Thus, no literature data was included in Figure 11(b) and (d).

the mass fraction and enthalpy, that is, $\frac{\eta_y}{\eta_h}$, represents the Le_t. Figure 12(b) and (d) plots the Le_t along the radial direction where the Gaussian coefficient ratio was obtained by averaging the ratios at different locations (Table 4).

Despite the considerable scattering in Figures 9 and 11 among individual decay rates, the calculated Le_t collapse into a rather tight band. Le_t is shown to increase with release temperature and decrease with Reynolds number. The dependence of Le_t on release temperature and Reynolds number appears to be stronger in the axial direction than in the radial direction, even discarding the 35 K and 48 K cases. On the other hand, at room temperature, Le_t in both directions reaches approximately 0.95, close to the typically assumed value of 1 in CFD simulations (Giannissi and Venetsanos, 2018; Saini *et al.*, 2024). Similar to our 35 and 50 K cases, the Le_t derived from the Sandia experiments are also well below 1, which is worth exploring in future work. A smaller Le_t, for example, 0.85, has been used in previous simulations of cryogenic hydrogen release (Giannissi *et al.*, 2021).

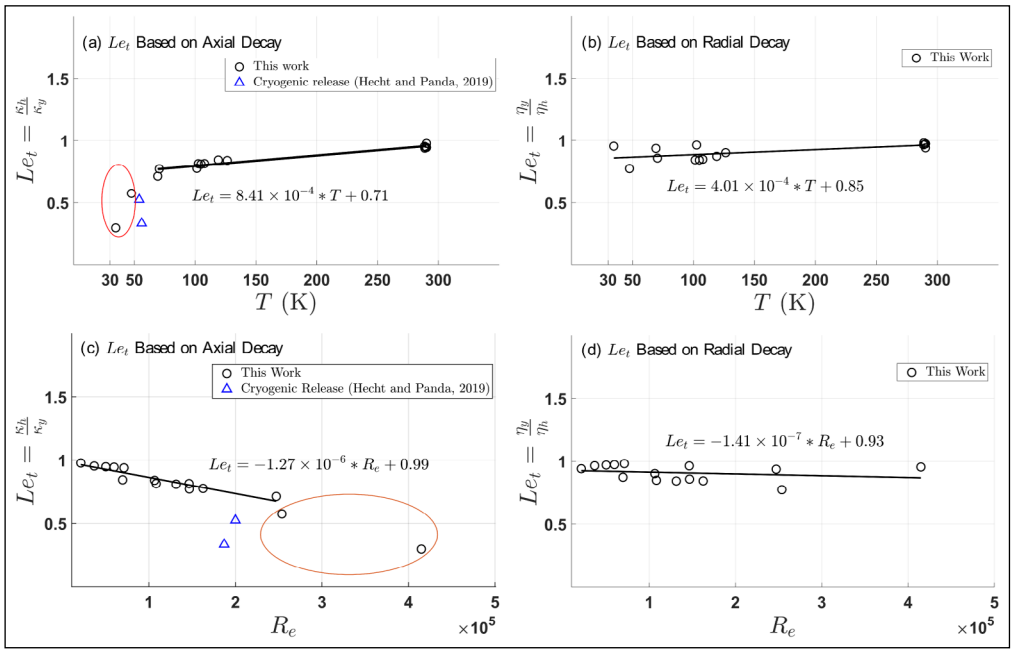

Figure 12 Le_t as a function of the release temperature, based on **(a)** the ratio of axial decay rates for enthalpy and mass fraction, and **(b)** the ratio of radial decay rates for mass fraction and enthalpy. The Le_t fitting for release temperature at 70 K or higher (35 and 50 K neglected and circled in red). Same Le_t plotted as a function of jet Reynolds number in **(c)** and **(d)**. Experiment data from this work (black circle), literature data (blue triangle) (Hecht and Panda, 2019).

The experimentally determined Le_t can be used to estimate Pr_t and Sc_t using the velocity decay rate from the CFD simulation. An example result for the 103 K/506 KPa release case is shown in Table 5, using the CFD method reported in Saini *et al.* (2024). The Pr_t is calculated to be 0.96 along the axial direction and 0.67 along the radial direction. This indicates that the transport of enthalpy and momentum is at a similar rate in the axial direction, but that enthalpy is transported faster than momentum in the radial direction, which can be explained by the stronger axial momentum. The Prandtl numbers (*Pr*) based on molecular properties are approximately 0.75 for air and 0.68 for hydrogen between 100 and 300 K, which is similar to Pr_t in the radial direction. This suggests that the radial decay is largely controlled by molecular diffusion, which is supported by Figure 11 where the jet Reynolds number shows little impact on the radial decay rates.

Table 5 Turbulent Pr_t and Sc_t estimation for release at 103 K, 506 KPa.

PARAMETERS		VALUE
Axial decay rate	Mass fraction κ_y	0.199 (measured)
	Enthalpy κ_h	0.162 (measured)
	Velocity κ_v	0.156 (CFD)
Axial turbulent parameters	$Le_t = \frac{\kappa_h}{\kappa_y}$	0.81 (measured)
	$Pr_t = \frac{\kappa_v}{\kappa_h}$	0.96 (calculated using CFD)
	$Sc_t = \frac{\kappa_v}{\kappa_y}$	0.78 (calculated using CFD)

(Contd.)

PARAMETERS		VALUE
Radial decay rate	Mass fraction η_y	40.5 (measured)
	Enthalpy η_h	41.5 (measured)
	Velocity η_v	62 (CFD)
Radial turbulent parameters	$Le_t = \frac{\eta_y}{\eta_h}$	0.96 (measured)
	$Pr_t = \frac{\eta_h}{\eta_v}$	0.67 (calculated using CFD)
	$Sc_t = \frac{\eta_y}{\eta_v}$	0.65 (calculated using CFD)

3.4 TWO-DIMENSIONAL HYDROGEN CONCENTRATION CONTOUR

To evaluate the impact of release temperature on the size of flammable envelope, two-dimensional contours of hydrogen concentrations are constructed using the centreline measurements and the average Gaussian function fitted from the radial measurements at the same condition. Figure 13 shows the results for release temperature at 35–290 K at a fixed release pressure of 300 kPa, indicating a larger hydrogen concentration contour as the release temperature decreases (where mass flow rate increases).

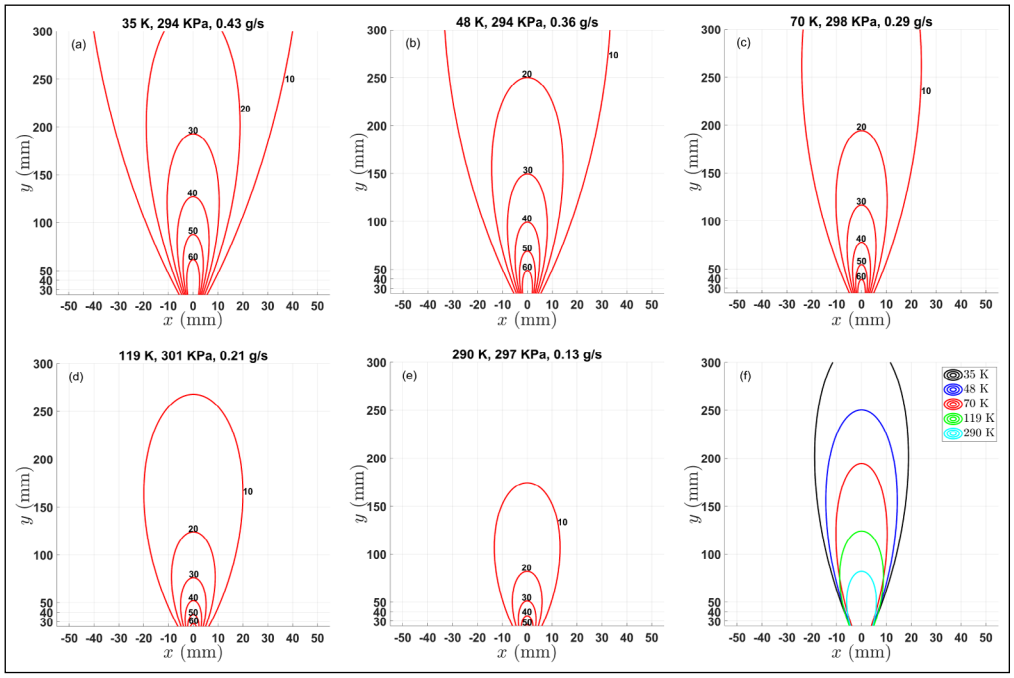

Figure 13 Hydrogen mole fraction (%) contour at different release temperatures and a fixed release pressure of 300 KPa: **(a)** 35 K, **(b)** 48 K, **(c)** 70 K, **(d)** 119 K, **(e)** 290 K and **(f)** contours of 20% H_2 mole fraction at different release temperatures.

Figure 14 shows the hydrogen concentration contour for release temperature at 35–289 K at a fixed mass flow rate of 0.43g/s, which also shows a larger hydrogen concentration contour at lower release temperature. The longer contour can be explained by the slower axial decay of colder jets, as shown in Figure 9. The wider contour apparently contradicts the faster radial decay of colder jets in Figure 11. However, the radial decay is relative to its centreline concentration, which decays more slowly with colder jets. The combination of the two effects results in a longer and wider contour for cold jets, indicating a deeper jet penetration as well as a higher volume of flammable gas, both suggesting a larger separation distance compared to the room temperature release at comparable release pressure or mass flow rate.

3.5 ADIABATIC MIXING

The adiabatic mixing assumption is examined using the cryogenic release data (35–126 K) in this work. The mixing equation is written as

$$X_{H_2,calculated} = \frac{\overline{C}_{p_{H_2},mix} T_{mix} - \overline{C}_{p_{air,\infty}} T_\infty}{\overline{C}_{p_{H_2,e}} T_e + \overline{C}_{p_{air,mix}} T_{mix} - \overline{C}_{p_{air,\infty}} T_\infty - \overline{C}_{p_{H_2,mix}} T_{mix}} \quad (7)$$

DOI: 10.58895/hysafe.79

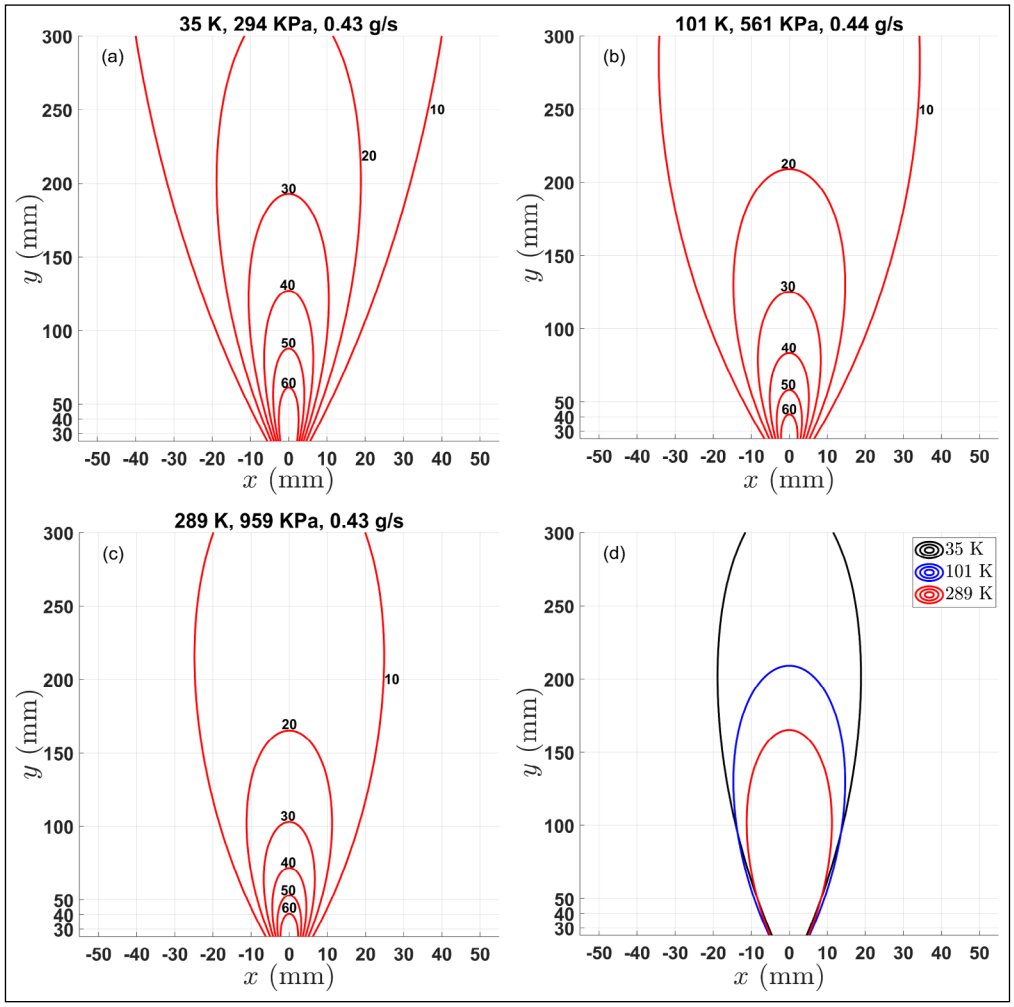

Figure 14 Hydrogen concentration contour at different release temperatures and a fixed mass flow rate of 0.43 g/s: **(a)** 35 K, **(b)** 101 K, **(c)** 289 K and **(d)** contours of 20% H_2 mole fraction at different release temperatures.

where X_{H2} is hydrogen molar fraction and T_mix is the mixture temperature. $\bar{C}_{p_i}$ is the molar-based specific heat and the subscript *e*, ∞ and *mix* indicating the value at the temperature of the nozzle exit, ambient and mixture, respectively.

Figure 15 shows both the experimentally measured hydrogen mole fraction ($X_{H2,measured}$) and the calculated hydrogen mole fraction ($X_{H2,calculated}$) using the adiabatic mixing equation (equation (7)). All data points generally collapse onto a straight line with a slope of 1.06, with some outliers at both ends of the measured range. At high H_2%, the deviation could be due to air condensation; at low H_2%, it could be due to the error in measuring small hydrogen concentrations (±2 vol%). Although this result proves adiabatic mixing is generally applicable to cryogenic jet mixing, an accurate correlation between species concentration and mixture temperature must take into account the deviation from the 1:1 fitting.

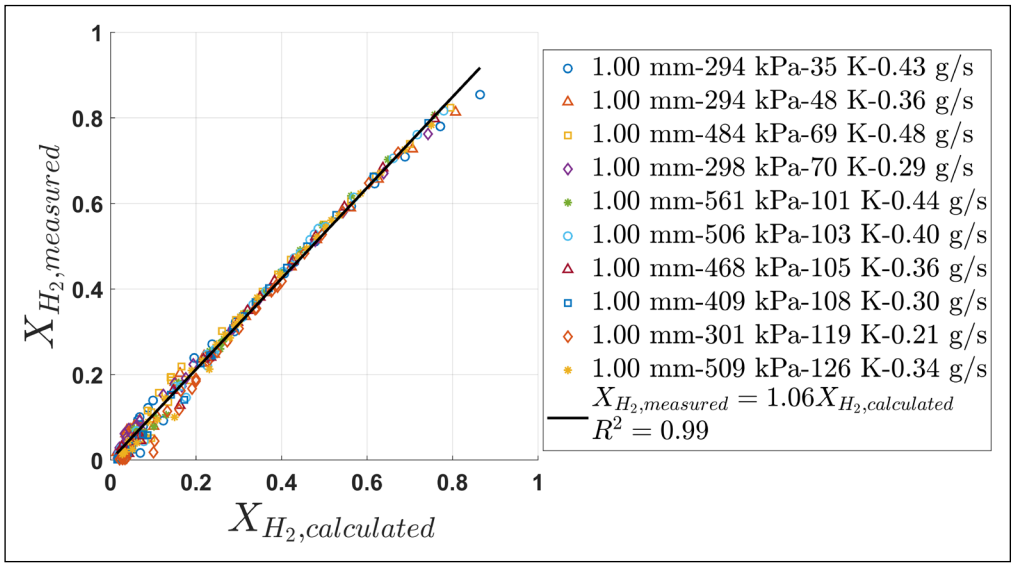

Figure 15 Examination of the applicability of adiabatic mixing to the cryogenic release experiments. $X_{H2,calculated}$ is from equation (7). Both axial and radial measurements are plotted; the black line is the linear fitting of all plotted data. A slope of 1 means perfect adiabatic mixing.

DOI: 10.58895/hysafe.79

3.5 COMPARISON WITH HYRAM SIMULATION

Simulation using HyRAM+ 6.0 (Ehrhart *et al.*, 2025) is conducted for all the cases investigated. The results for the release temperature sweep at 300 kPa are presented below. The remaining results are reported in the Supplementary Materials. To account for the presence of the sampling probe in the jet, simulation results are averaged over a circular cross-section of 1.5 mm diameter (corresponding to the probe inner diameter) for comparison with measurements. A revised HyRAM code has been published (Saini *et al.*, 2025) of which the simulation results are also included in the Supplementary Materials.

3.5.1 Axial molar fraction and temperature

Figure 16 compares the simulated hydrogen molar fraction and mixture temperature along the axial direction. HyRAM appears to underpredict both parameters at the same time, which is in contradiction with the adiabatic mixing discussed above; for example, a higher hydrogen concentration should lead to a lower gas temperature. The underprediction of mole fraction is more severe near the nozzle (less than 40 mm above the nozzle) at release temperatures below 70 K. One potential contributor might be the condensation of air components in this region, which could increase local gas temperature and hydrogen mole fraction simultaneously. Nevertheless, the overall HyRAM prediction for centreline concentration and temperature is satisfactory.

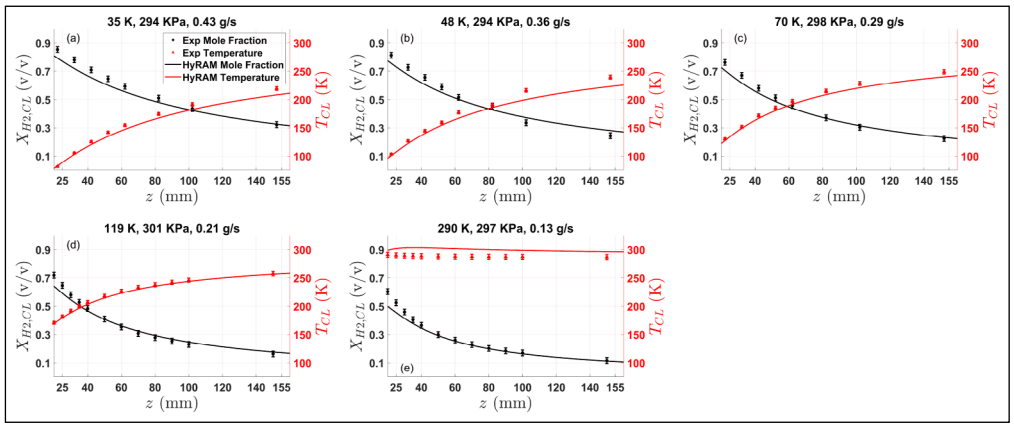

Figure 16 Comparison of measured and simulated centreline hydrogen molar fraction and mixture temperature at different release temperatures and a fixed release pressure of 300 kPa: **(a)** 35 K, **(b)** 48 K, **(c)** 70 K, **(d)** 119 K and **(e)** 290 K; symbols for experiment data and curves for HyRAM simulation; black for hydrogen mole fraction and red for mixture temperature.

3.5.2 Radial molar fraction and temperature

Figure 17 compares the measured and simulated radial decay for normalized hydrogen mole fraction and mixture temperature. The simulation reproduces the measured mole fraction and temperature well for the deep cryogenic release (35–70 K). The mixture temperature is almost constant for the room temperature release and therefore cannot be fitted by Gaussian functions. As the release temperature increases, larger discrepancies are observed for the 119 K and room temperature cases. These results indicate that HyRAM needs to improve the radial simulation for release temperatures above 100 K. Similar results are observed in other datasets reported in the Supplementary Materials.

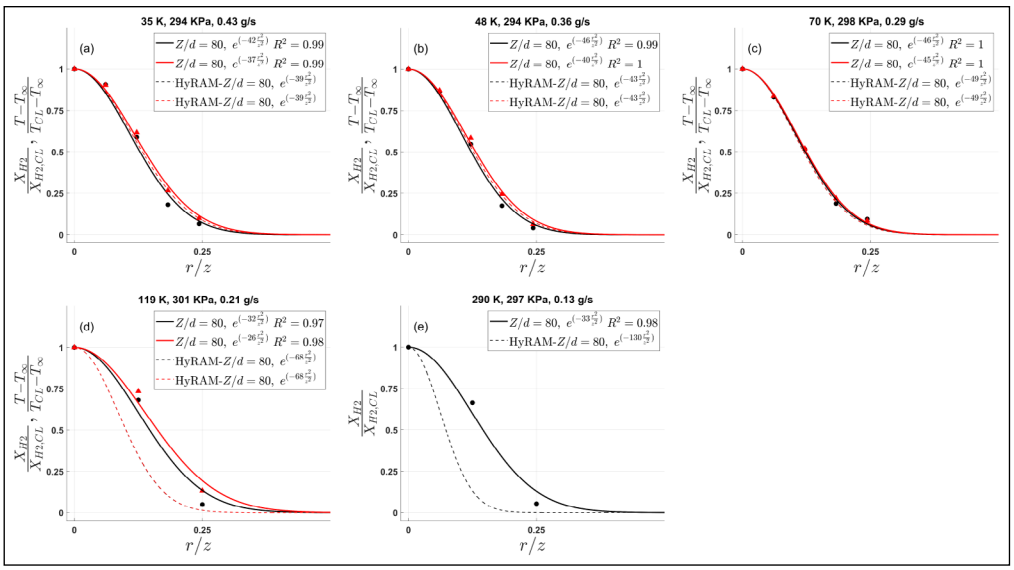

Figure 17 Comparison of the measured and simulated radial hydrogen mole fraction and mixture temperature at different release temperatures and a fixed release pressure of 300 kPa, **(a)** 35 K, **(b)** 48 K, **(c)** 70 K, **(d)** 119 K and **(e)** 290 K; solid lines are fitted from measurements (markers) and dashed lines represent results from the HyRAM+ 6.0 simulation; black for hydrogen mole fraction and red for mixture temperature.

The problem of simulating room temperature release has been reported with previous versions of HyRAM (Ehrhart *et al.*, 2021). Part of this can be attributed to some empirical constants being (over)tuned for deep cryogenic conditions. For example, the spreading ratio (λ) for the relative decay of velocity and mass fraction/temperature fields was reduced from 1.5 (version 2.0) to 1.16 (version 3.1 and later versions), which improved the simulation of cryogenic releases but worsened the simulation of room temperature cases (Ehrhart *et al.*, 2021). It is also noted that there is no differentiation of concentration and temperature decay in the HyRAM simulation.

4. CONCLUSIONS

This work investigates turbulent axisymmetric hydrogen jet mixing with ambient air in a controlled environment under systematically varied release conditions of 35–290 K, 300–950 KPa and 0.13–0.43 g/s. The hydrogen concentration and gas temperature were measured across the mixing jet using a movable sampling probe with two degrees of freedom. The decays along the axial and radial directions were analysed using Kleinstein's method. The major conclusions are as follows:

1. Under cryogenic release conditions, the axial decay rate of the hydrogen mass fraction and the mixture enthalpy, as described by κ_y and κ_h in the hyperbolic function (equation (1)), both decreased with decreasing release temperature, indicating slower axial mixing with a colder jet.
2. In the radial direction, the decay rate of the hydrogen mass fraction and the mixture enthalpy, as described by η_y and η_h in the Gaussian distribution function (equation (3)), both increased with decreasing release temperature, indicating faster radial mixing with a colder jet.
3. Combining the axial and radial effects, cryogenic hydrogen jets produced a longer and larger flammable envelope.
4. The turbulent Lewis number was estimated using κ_h/κ_y along the axial direction, and η_y/η_h along the radial direction, which greatly reduced the scattering among the individual decay rates. With decreasing release temperature, Le_t decreased in both axial and radial directions, whereas the axial Le_t depended more on release temperature. The room temperature value of Le_t returned to 0.95 in both directions.
5. The HyRAM simulation reproduced the axial and radial measurements reasonably in most cases, but the performance deteriorated with increasing release temperature. This is likely due to the identical, temperature-invariant decay rates assumed for hydrogen concentration and mixture temperature in the simulation.

These results demonstrated the slower decay with cryogenic jets and call for additional prudence in evaluating the consequence of liquid hydrogen leaks. Future work is therefore recommended on the velocity decay in cryogenic jets and the extension of Kleinstein's analysis to deep cryogenic conditions. This will help to provide key inputs (turbulent transport properties) to CFD simulations and low-order models.

ADDITIONAL FILE

The additional file for this article can be found as follows:

- **Supplementary Materials.** The measured hydrogen concentration and mixture temperature data are provided in the Supplementary Materials. Available at: https://doi.org/10.58895/hysafe.79.s1

FUNDING INFORMATION

We thank the Victorian High Education State Investment Fund, Fortescue Future Industries, Australian Renewable Energy Agency and Future Energy Export CRC for supporting this work. The Future Energy Exports CRC (www.fenex.org.au) is funded by the Australian Government's Cooperative Research Centre Program. This is FEnEx CRC Document 2026/24.RP2.0173-FNX-MILE0895.

COMPETING INTERESTS

The authors have no competing interests to declare.

AUTHOR CONTRIBUTIONS

Qiang Ge: Investigation, formal analysis, writing—original manuscript. Zhenbiao Zhou: Investigation, methodology, formal analysis, supervision, writing—review and editing. Daniel Creedon: Methodology, writing—review and editing. Yi Yang: Conceptualization, formal analysis, methodology, funding acquisition, project administration, supervision, writing—review and editing. Michael Brear: Conceptualization, methodology, funding acquisition, writing—review and editing. Deepak Saini: Formal analysis, writing—review and editing. Joe Berry: Formal analysis, funding acquisition, writing—review and editing. Mohsen Talei: Formal analysis, funding acquisition, writing—review and editing. Richard Sandberg: Formal analysis, funding acquisition, writing—review and editing. Melissa Kozul: Formal analysis, funding acquisition, writing—review and editing.

AUTHOR AFFILIATIONS

Qiang Ge orcid.org/0009-0001-1602-1530
Department of Mechanical Engineering, University of Melbourne, AU

Zhenbiao Zhou orcid.org/0000-0003-4204-3108
Department of Mechanical Engineering, University of Melbourne, AU

Daniel Creedon orcid.org/0000-0003-2912-3381
Department of Mechanical Engineering, University of Melbourne, AU

Yi Yang orcid.org/0000-0003-4145-5039
Department of Mechanical Engineering, University of Melbourne, AU

Michael J. Brear orcid.org/0000-0002-1646-2926
Department of Mechanical Engineering, University of Melbourne, AU

Deepak Saini orcid.org/0000-0003-4499-824X
Department of Chemical Engineering, University of Melbourne, AU

Joseph D. Berry orcid.org/0000-0002-0961-7782
Department of Chemical Engineering, University of Melbourne, AU

Mohsen Talei orcid.org/0000-0001-5923-2461
Department of Mechanical Engineering, University of Melbourne, AU

Richard D. Sandberg orcid.org/0000-0001-5199-3944
Department of Mechanical Engineering, University of Melbourne, AU

Melissa Kozul orcid.org/0000-0001-9881-1677
Department of Mechanical Engineering, University of Melbourne, AU

REFERENCES

Bilger, R.W. and **Beck, R.E.** (1975) 'Further experiments on turbulent jet diffusion flames', *Symposium (International) on Combustion*, 15, pp. 541–552. Available at: https://doi.org/10.1016/S0082-0784(75)80326-2

Birch, A., Brown, D., Dodson, M. and **Swaffield, F.** (1984) 'The structure and concentration decay of high pressure jets of natural gas', *Combustion Science and Technology*, 36, pp. 249–261. Available at: https://doi.org/10.1080/00102208408923739

Birch, A., Hughes, D. and **Swaffield, F.** (1987) 'Velocity decay of high pressure jets', *Combustion Science and Technology*, 52, pp. 161–171. Available at: https://doi.org/10.1080/00102208708952575

Chen, C.J. and **Rodi, W.** (1980) *Vertical turbulent buoyant jets: a review of experimental data*. New York: Pergamon Press.

Corrsin, S. and **Uberoi, M.** (1949) *Further experiments on the flow and heat transfer in a heated turbulent air jet*. Hampton, VA: National Advisory Committee for Aeronautics.

Courant, R. and **Friedrichs, K.O.** (1948) *Supersonic flow and shock waves*. New York: Interscience Publishers.

Ehrhart, B.D., Hecht, E.S. and **Mohmand, J.A.** (2021) Validation and Comparison of HyRAM Physics Models. Albuquerque, NM: Sandia National Laboratories (SNL-NM). Available at: https://doi.org/10.2172/1813659

Ehrhart, B.D., Hecht, E.S., Devin, M.C., Groth, K.M., Reynolds, J.T., Blaylock, M.L., Carrier, E.E. and **Schroeder, B.B.** (2025) *Hydrogen plus other alternative fuels risk assessment models (HyRAM+) technical reference manual (V.6.0)*. Albuquerque, NM: Sandia National Laboratories (SNL-NM).

Ewan, B.C.R. and **Moodie, K.** (1986) 'Structure and velocity measurements in underexpanded jets. *Combustion Science and Technology*, 45, pp. 275–288. Available at: https://doi.org/10.1080/00102208608923857

Ferri, A., Libby, P.A. and **Zakkay, V.** (1964) 'Theoretical and experimental investigation of supersonic combustion', in C. Ferrari (ed.) *High temperatures in aeronautics*. New York: Elsevier. pp. 55–118. Available at: https://doi.org/10.1016/B978-0-08-010558-1.50011-6

Franquet, E., Perrier, V., Gibout, S. and **Bruel, P.** (2015) 'Free underexpanded jets in a quiescent medium: a review', *Progress in Aerospace Sciences*, 77, pp. 25–53. Available at: https://doi.org/10.1016/j.paerosci.2015.06.006

Friedrich, A., Breitung, W., Stern, G., Veser, A., Kuznetsov, M., Fast, G., Oechsler, B., Kotchourko, N., Jordan, T., Travis, J.R., Xiao, J., Schwall, M. and **Rottenecker, M.** (2012) 'Ignition and heat radiation of cryogenic hydrogen jets', *International Journal of Hydrogen Energy*, 37, pp. 17589–17598. Available at: https://doi.org/10.1016/j.ijhydene.2012.07.070

Giannissi, S. and **Venetsanos, A.** (2018) 'Study of key parameters in modeling liquid hydrogen release and dispersion in open environment', *International Journal of Hydrogen Energy*, 43, pp. 455–467. Available at: https://doi.org/10.1016/j.ijhydene.2017.10.128

Giannissi, S.G., Venetsanos, A.G., Cirrone, D., Molkov, V.V., Ren, Z., Wen, J.X., Friedrich, A. and **Veser, A.** (2021) 'Cold hydrogen blowdown release: an inter-comparison study', *9th international conference on Hydrogen Safety (ICHS 2021)*. Edinburgh, UK.

Hecht, E.S. and **Panda, P.P.** (2019) 'Mixing and warming of cryogenic hydrogen releases', *International Journal of Hydrogen Energy*, 44, pp. 8960–8970. Available at: https://doi.org/10.1016/j.ijhydene.2018.07.058

Hu, R., Chen, Y., Wu, J. and **Tian, S.** (2023) 'The influence of gas models on numerical simulations of cryogenic flow', *Aerospace*, 10, p. 986. Available at: https://doi.org/10.3390/aerospace10120986

Kent, J.H. and **Bilger, R.W.** (1973) 'Turbulent diffusion flames', *Symposium (International) on Combustion*, 14, pp. 615–625. Available at: https://doi.org/10.1016/S0082-0784(73)80058-X

Kleinstein, G. (1964) 'Mixing in turbulent axially symmetric free jets', *Journal of Spacecraft and Rockets*, 1, pp. 403–408. Available at: https://doi.org/10.2514/3.27669

Lachance, J.L., Houf, W.G., Fluer, L. and **Middleton, B.** (2009) 'Analyses to support development of risk-informed separation distances for hydrogen codes and standards', *SAND2009-0874*. Sandia National Laboratories.

Lemmon, E., Huber, M. and **McLinden, M.** (2013) 'NIST standard reference database 23: reference fluid thermodynamic and transport properties-REFPROP, version 9.1'. National Standard Reference Data Series (NIST NSRDS). National Institute of Standards and Technology, Gaithersburg, MD.

Li, X., Chen, M., Wang, Y., Hu, J., Sun, Z., Christopher, D.M. and **Cheng, L.** (2018) 'Measurements of concentration decays in underexpanded jets through rectangular slot nozzles', *International Journal of Hydrogen Energy*, 43, pp. 9884–9893. Available at: https://doi.org/10.1016/j.ijhydene.2018.04.022

Li, X., Yao, C., Egbert, S.C., He, Q., Zhao, Z., Christopher, D.M. and **Hecht, E.S.** (2023) 'Self-similar characteristics of underexpanded, cryogenic hydrogen and methane jets', *International Journal of Hydrogen Energy*, 48, pp. 4104–4117. Available at: https://doi.org/10.1016/j.ijhydene.2022.10.117

Lupant, D., Pesenti, B. and **Lybaert, P.** (2010) 'Influence of probe sampling on reacting species measurement in diluted combustion', *Experimental Thermal and Fluid Science*, 34, pp. 516–522. Available at: https://doi.org/10.1016/j.expthermflusci.2009.11.004

Matheis, J., Mller, H., Hickel, S. and **Pfitzner, M.** (2020) 'Large-eddy simulation of cryogenic jet injection at supercritical pressures', in J. Bellan (ed.) *High-pressure flows for propulsion applications*. Reston, VA: American Institute of Aeronautics and Astronautics. pp. 531–570. Available at: https://doi.org/10.2514/5.9781624105814.0531.0570

Molkov, V. (2012) 'Hydrogen safety engineering: the state-of-the-art and future progress', in A. Sayigh (ed.) *Comprehensive renewable energy*. Oxford, UK: Elsevier. pp. 97–129. Available at: https://doi.org/10.1016/B978-0-08-087872-0.00418-2

NFPA (2023) *NFPA 2: hydrogen technologies code*. Quincy, MA: National Fire Protection Association.

Okabayashi, K., Tagashira, K., Kawazoe, K., Takeno, K., Asahara, M., Hayashi, A.K. and **Komori, M.** (2019) 'Non-steady characteristics of dispersion and ignitability for high-pressurized hydrogen jet discharged from a pinhole', *International Journal of Hydrogen Energy*, 44, pp. 9071–9079. Available at: https://doi.org/10.1016/j.ijhydene.2018.05.047

Olshefski, K., Collins, A., Coulon, T., Lowe, T. and **Ng, W.** (2022) 'Development of an anisokinetic particle sampling probe for use in a gas turbine engine compressor', *Frontiers in Mechanical Engineering*, 8:951986. Available at: https://doi.org/10.3389/fmech.2022.951986

Panda, P.P. and **Hecht, E.S.** (2017) 'Ignition and flame characteristics of cryogenic hydrogen releases', *International Journal of Hydrogen Energy*, 42, pp. 775–785. Available at: https://doi.org/10.1016/j.ijhydene.2016.08.051

Richards, C.D. and **Pitts, W.M.** (1993) 'Global density effects on the self-preservation behaviour of turbulent free jets', *Journal of Fluid Mechanics*, 254, pp. 417–435. Available at: https://doi.org/10.1017/S0022112093002204

Ruffin, E., Mouilleau, Y. and **Chaineaux, J.** (1996) 'Large scale characterization of the concentration field of supercritical jets of hydrogen and methane', *Journal of Loss Prevention in the Process Industries*, 9, pp. 279–284. Available at: https://doi.org/10.1016/0950-4230(96)00018-6

Ruggles, A.J. (2015) 'Statistically advanced, self-similar, radial probability density functions of atmospheric and under-expanded hydrogen jets', *Experiments in Fluids*, 56, pp. 1–25. Available at: https://doi.org/10.1007/s00348-015-2074-8

Ruggles, A.J. and **Ekoto, I.W.** (2012) 'Ignitability and mixing of underexpanded hydrogen jets', *International Journal of Hydrogen Energy*, 37, pp. 17549–17560. Available at: https://doi.org/10.1016/j.ijhydene.2012.03.063

Saini, D., Talei, M., Yang, Y., Sandberg, R.D. and **Berry, J.D.** (2024) 'Effect of storage conditions on the characteristics of cryogenic hydrogen jet dispersion', *International Journal of Hydrogen Energy*, 67, pp. 1–15. Available at: https://doi.org/10.1016/j.ijhydene.2024.04.040

Saini, D., Talei, M., Yang, Y., Sandberg, R.D. and **Berry, J.D.** (2025) 'Improving low-order modelling of cryogenic hydrogen releases', *International Journal of Hydrogen Energy*, 105, pp. 417–426. Available at: https://doi.org/10.1016/j.ijhydene.2025.01.148

Schefer, R., Evans, G., Zhang, J., Ruggles, A. and **Greif, R.** (2011) 'Ignitability limits for combustion of unintended hydrogen releases: experimental and theoretical results', *International Journal of Hydrogen Energy*, 36, pp. 2426–2435. Available at: https://doi.org/10.1016/j.ijhydene.2010.04.004

Schlichting, H. and **Gersten, K.** (2017) 'exact solutions of the Navier–Stokes equations' in H. Schlichting and K. Gersten (eds.) *Boundary-Layer theory*. Berlin, Heidelberg: Springer. pp. 101–142. Available at: https://doi.org/10.1007/978-3-662-52919-5_5

Shapiro, A.H. (1953) *The dynamics and thermodynamics of compressible fluid flow*. New York: Ronald Press.

So, R. and **Aksoy, H.** (1993) 'On vertical turbulent buoyant jets', *International Journal of Heat and Mass Transfer*, 36, pp. 3187–3200. Available at: https://doi.org/10.1016/0017-9310(93)90003-O

Takeno, K., Okabayashi, K., Kouchi, A., Misaka, N. and **Hashiguchi, K.** (2017) 'Concentration fluctuation and ignition characteristics during atmospheric diffusion of hydrogen spouted from high pressure storage', *International Journal of Hydrogen Energy*, 42, pp. 15426–15434. Available at: https://doi.org/10.1016/j.ijhydene.2017.04.062

Traxinger, C., Banholzer, M. and **Pfitzner, M.** (2018) 'Real-gas effects and phase separation in underexpanded jets at engine-relevant conditions', 2018 AIAA Aerospace Sciences Meeting, 2018. Reston, VA: American Institute of Aeronautics and Astronautics. Available at: https://doi.org/10.2514/6.2018-1815

Veser, A., Kuznetsov, M., Fast, G., Friedrich, A., Kotchourko, N., Stern, G., Schwall, M. and **Breitung, W.** (2011) 'The structure and flame propagation regimes in turbulent hydrogen jets', *International Journal of Hydrogen Energy*, 36, pp. 2351–2359. Available at: https://doi.org/10.1016/j.ijhydene.2010.03.123

Yuceil, K. and **Otugen, M.** (2002) 'Scaling parameters for underexpanded sonic jets' *Physics of Fluids*, 14, pp. 4206–4215. Available at: https://doi.org/10.1063/1.1513796

Yue, M., Lambert, H., Pahon, E., Roche, R., Jemei, S. and **Hissel, D.** (2021) 'Hydrogen energy systems: a critical review of technologies, applications, trends and challenges', *Renewable and Sustainable Energy Reviews*, 146, p. 111180. Available at: https://doi.org/10.1016/j.rser.2021.111180

TO CITE THIS ARTICLE:
Ge, Q., Zhou, Z., Creedon, D., Yang, Y., Brear, M.J., Saini, D., Berry, J.D., Talei, M., Sandberg, R.D. and Kozul, M. (2026) 'Impact of Release Temperature on Hydrogen Jet Mixing with Ambient Air', *Hydrogen Safety*, 3(1), pp. 284–304. Available at: https://doi.org/10.58895/hysafe.79

Submitted: 14 May 2026
Accepted: 24 August 2026
Published: 10 September 2026

Hydrogen Safety is a peer-reviewed open access journal published by KIT Scientific Publishing.

KIT Scientific Publishing